

Drive-KD: Multi-Teacher Distillation for VLMs in Autonomous Driving

Weitong Lian^{* 1} Zecong Tang^{* † 1} Haoran Li^{* 1} Tianjian Gao¹ Yifei Wang¹
 Xixu Wang¹ Lingyi Meng¹ Tengju Ru¹ Zhejun Cui¹ Yichen Zhu¹ Hangshuo Cao¹
 Qi Kang¹ Tianxing Chen² Yusen Qin³ Kaixuan Wang² Yu Zhang^{‡ 1}

Abstract

Autonomous driving is an important and safety-critical task, and recent advances in LLMs/VLMs have opened new possibilities for reasoning and planning in this domain. However, large models demand substantial GPU memory and exhibit high inference latency, while conventional supervised fine-tuning (SFT) often struggles to bridge the capability gaps of small models. To address these limitations, we propose Drive-KD, a framework that decomposes autonomous driving into a “perception–reasoning–planning” triad and transfers these capabilities via knowledge distillation. We identify layer-specific attention as the distillation signal to construct capability-specific single-teacher models that outperform baselines. Moreover, we unify these single-teacher settings into a multi-teacher distillation framework and introduce asymmetric gradient projection to mitigate cross-capability gradient conflicts. Extensive evaluations validate the generalization of our method across diverse model families and scales. Experiments show that our distilled InternVL3-1B model, with 42x less GPU memory and 11.4x higher throughput, achieves better overall performance than the pretrained 78B model from the same family on DriveBench, and surpasses GPT-5.1 on the planning dimension, providing insights toward efficient autonomous driving VLMs.

1. Introduction

Autonomous driving is a highly complex domain with high safety requirements (Zhao et al., 2024). Classical autonomous driving solutions mainly follow two paradigms

(Yurtsever et al., 2020). One is a modular pipeline that decomposes object detection, tracking, behavior prediction, and trajectory planning into separate submodules (Vougioukas, 2019; Paden et al., 2016; Badue et al., 2021), and the other is an end-to-end learning paradigm that directly maps sensor inputs to control commands or semantic representations (Bojarski et al., 2016; Tampuu et al., 2020; Chen et al., 2024b). Despite their progress, both paradigms have key limitations. Modular pipelines often accumulate errors across stages, while end-to-end models remain hard to interpret and can be brittle under complex environments (Badue et al., 2021; Pan et al., 2024; Chen et al., 2024b).

In recent years, the rapid progress of large language models (LLMs) has shown that LLMs can follow instructions and perform chain-of-thought reasoning, and leverage rich world knowledge (Achiam et al., 2023; Bai et al., 2023; Liu et al., 2024). Furthermore, vision-language models (VLMs) demonstrate strong capabilities in zero-shot transfer and language-based reasoning, highlighting their potential for autonomous driving (Hurst et al., 2024; Wang et al., 2024b; Team, 2025; Chen et al., 2024c). A number of recent studies have begun to adapt VLMs to autonomous driving, ranging from open-loop scene understanding to language-guided closed-loop driving systems, but they still face challenges in reliability and real-time performance (Tian et al., 2024; Sima et al., 2025; Shao et al., 2024).

Knowledge distillation (KD) transfers knowledge from large models to small ones, enabling efficient deployment on resource-constrained edge devices (Xu et al., 2024b; Moslemi et al., 2024). However, current approaches lack systematic studies on distillation signal selection in autonomous driving, which provides limited guidance on where to apply supervision (Feng et al., 2024; Yang et al., 2025). Moreover, many works treat driving capabilities as parallel objectives, ignoring their sequential dependencies (Tian et al., 2024; Shao et al., 2024). When multiple distillation objectives are jointly optimized, a common practice is to aggregate them with a fixed or heuristic weighted sum, which can improve one capability at the cost of degrading others (Pham et al., 2023; Zhang et al., 2023). Furthermore, some distillation studies are restricted to a single scale or model family, making it difficult to validate generality (Feng

^{*} Equal contribution.

[†] Project leader.

[‡] Corresponding author.

¹ Zhejiang University, Hangzhou, China ² The University of Hong Kong, Hong Kong, China ³ D-Robotics, Shenzhen, China.

Preprint. January 30, 2026.

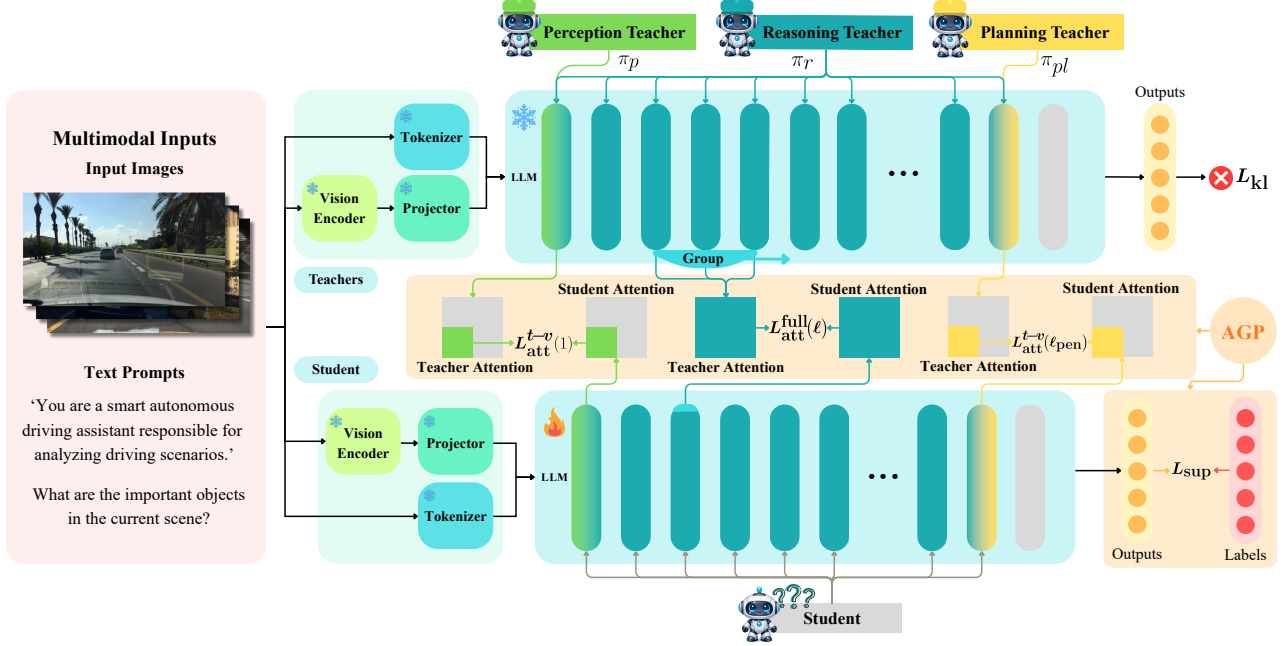


Figure 1. Drive-KD multi-teacher distillation framework. Three teachers distill attention at different student layers: Perception/Planning uses first-layer/penultimate-layer cross-modal attention; Reasoning uses grouped-matching intermediate-layer full attention. The student is also trained with hard-label supervision at the output. We apply AGP to mitigate cross-capability gradient conflicts.

et al., 2024; Zhong et al., 2024; Chen et al., 2024a).

To address these limitations, we propose Drive-KD (Figure 1), a multi-teacher distillation framework for small-scale VLMs. Following the human driving thought process, we decompose autonomous driving into a sequential triad of capabilities, “perception–reasoning–planning”, where later stages build on earlier-stage information. Based on this capability decomposition, we first investigate layer selection strategies from both representation and capability perspectives. We then identify suitable supervision signals for capability transfer by comparing their dispersion, and analyze why output-distribution alignment is not suitable for autonomous driving tasks.

Based on these findings, we systematically study distillation recipes for the three capabilities in autonomous driving, achieving capability scores that significantly outperform both pretrained and SFT baselines. These results further validate the layer and signal selection principles identified in our initial analyses. Moreover, we build Drive-KD as a multi-teacher distillation framework over the three capabilities, and apply asymmetric gradient projection (AGP) to mitigate gradient conflicts, yielding stronger capabilities in the small model. We further demonstrate the generality of Drive-KD across model scales and different model families.

We summarize our contributions as follows:

- First, we conduct the first systematic study of distilla-

tion design for autonomous driving VLMs, providing choices for distillation layers and supervision signals, and highlighting the limitations of output-distribution alignment for autonomous driving.

- Second, we derive the single-teacher distillation recipes for each capability and show stable improvements over pretrained and SFT baselines, which further validates our distillation signal selection principles.
- Third, we develop Drive-KD as a multi-teacher distillation framework and introduce AGP to alleviate cross-capability gradient conflicts. We further verify the generality of Drive-KD across model scales and different model families.
- Fourth, we demonstrate that our distilled InternVL3-1B achieves strong efficiency–performance trade-offs—requiring $\sim 42 \times$ less GPU memory and delivering $\sim 11.4 \times$ higher throughput—while outperforming the pretrained 78B model from the same family on DriveBench and surpassing GPT-5.1 on planning.

2. Related Work

2.1. LLM / VLM in Autonomous Driving

The rapid progress of LLMs has accelerated the development of multimodal models (Zhao et al., 2023; Zhang et al., 2024). Building on this trend, VLMs have emerged and

show strong general capabilities in complex scene description, visual question answering, and multi-step reasoning (Lu et al., 2025; Zhu et al., 2024; Wang et al., 2024b), which naturally match the requirements of autonomous driving (Zhou et al., 2024; You et al., 2026; Guo et al., 2024; Li et al., 2025a). Recent efforts explore VLM-based scene description and hierarchical planning, employ structured VQA for reasoning, and develop end-to-end driving systems with language-grounded low-level controls (Tian et al., 2024; Sima et al., 2025; Shao et al., 2024; Xu et al., 2024c; Xu et al.; Hwang et al., 2025). However, current VLMs still suffer from issues such as hallucination, unstable decision-making, and poor real-time performance (Zhang et al., 2024; Guan et al., 2024; Li et al., 2025c; Tang et al., 2026).

2.2. Distillation for LLM / VLM

KD aims to transfer knowledge from a large teacher model to a smaller student model, improving the student’s performance under limited capacity (Xu et al., 2024a; Gou et al., 2021). It was originally dominated by output distribution alignment (Hinton et al., 2015). In the era of LLMs, KD has gradually expanded to richer forms of supervision beyond outputs (Li et al., 2023; Wang et al., 2024a; Pan et al., 2021). For VLMs, distillation needs to compress not only language modeling ability but also transfer cross-modal alignment and fusion (Feng et al., 2024; Gu et al., 2025; Li et al., 2025b). Accordingly, recent works combine output-level alignment with internal-signal distillation and adopt techniques such as multi-teacher distillation to convey finer-grained information (Li et al., 2023; Wang et al., 2024a). These VLM-oriented distillation methods have been widely applied to VQA compression and multimodal instruction following (Tian et al., 2025; Cao et al.; Neo et al., 2025). However, principled strategies for choosing distillation signals and coordinating distillation across tasks remain unclear (Liang et al., 2023; Wang et al., 2024a; Mansourian et al., 2025).

3. Methodology

3.1. Preliminary

We categorize driving capabilities into three sequential capabilities: perception, reasoning, and planning. Perception aims to identify semantic cues that form the basis for subsequent reasoning. Reasoning leverages these cues to infer relations and constraints among the environment. Planning then leverages the inferred information to determine safe driving actions. We aim to distill the three capabilities from a large teacher to a small student VLM.

3.2. Distillation Signal Selection

We investigate (i) the appropriate layers for distilling each capability and (ii) the specific signals to distill within the

selected layers. In addition, we revisit output-distribution alignment and analyze its limitations for autonomous driving. In our studies, we sample 1,000 images, and each image contains multiple questions under each capability. Figure 2 summarizes these analyses and supports our algorithm design. Appendix A.1–A.4 collects the extended layer-wise similarity, intra-consistency, dispersion, and KL analyses.

3.2.1. WHERE TO DISTILL: LAYER SELECTION

Distilling all layers is costly and often unnecessary: different layers encode different functions, and forcing the student to match the teacher everywhere can introduce redundant or even conflicting supervision (Liang et al., 2023). Instead, we select a small set of target layers that are most informative for each driving capability. We select distillation layers from two complementary views. From a representation view, we pick layers with strong representation change and clear cross-modal interaction. From a capability view, we use capability-wise intra-consistency to find layers with stable capability features across images.

Representation view. We use two layer-wise metrics: adjacent-layer cosine similarity of hidden states and within-layer vision–text cosine similarity. These metrics are computed on the sampled pre-study set. For Transformer layers $\ell = 1, \dots, N$, let hidden states be $\mathbf{H}^{(\ell)} \in \mathbb{R}^{B \times L \times D}$, with token vectors $\mathbf{h}_{b,i}^{(\ell)} \in \mathbb{R}^D$ at position i of sample b . Treating the input embeddings as layer $\ell = 0$, we write $\mathbf{H}^{(0)} \in \mathbb{R}^{B \times L \times D}$ with token vectors $\mathbf{h}_{b,i}^{(0)}$, and the penultimate layer index is $\ell_{\text{pen}} = N - 1$. We define adjacent-layer similarity as cosine similarity at matched token positions, averaged over samples and token indices:

$$S^{(\ell)} = \mathbb{E}_{b,i} \left[\frac{\mathbf{h}_{b,i}^{(\ell)} \cdot \mathbf{h}_{b,i}^{(\ell+1)}}{\|\mathbf{h}_{b,i}^{(\ell)}\|_2 \|\mathbf{h}_{b,i}^{(\ell+1)}\|_2} \right], \quad \ell = 0, \dots, N - 1. \quad (1)$$

To measure intra-layer vision–text similarity, we split tokens into vision and text segments and mean-pool each segment:

$$\bar{\mathbf{v}}_b^{(\ell)} = \frac{1}{|\mathcal{V}_b|} \sum_{i \in \mathcal{V}_b} \mathbf{h}_{b,i}^{(\ell)}, \quad \bar{\mathbf{t}}_b^{(\ell)} = \frac{1}{|\mathcal{T}_b|} \sum_{j \in \mathcal{T}_b} \mathbf{h}_{b,j}^{(\ell)}. \quad (2)$$

Here \mathcal{V}_b and \mathcal{T}_b denote the index sets of visual and text tokens for sample b . We then compute cosine similarity:

$$C^{(\ell)} = \mathbb{E}_b \left[\frac{\bar{\mathbf{v}}_b^{(\ell)} \cdot \bar{\mathbf{t}}_b^{(\ell)}}{\|\bar{\mathbf{v}}_b^{(\ell)}\|_2 \|\bar{\mathbf{t}}_b^{(\ell)}\|_2} \right]. \quad (3)$$

Across all models, $S^{(0)}$ is low while $S^{(1)}$ rises sharply, and $S^{(N-1)}$ drops relative to $S^{(N-2)}$, highlighting major representation changes near Layer 1 and ℓ_{pen} . Meanwhile, $C^{(\ell)}$ exhibits a clear fusion peak near the penultimate layer (ℓ_{pen}), indicating strong vision–text interaction. These results suggest that Layer 1 and Layer ℓ_{pen} serve as key

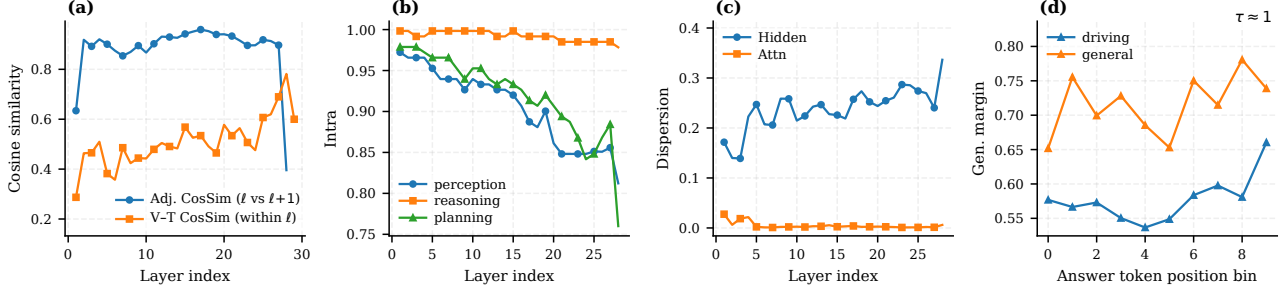


Figure 2. Pre-study summary for InternVL3-8B: (a) layer-wise distillation alignment measured by cosine similarity (adjacent-layer and within-layer vision-text), (b) capability-wise intra-group similarity across layers, (c) layer-wise dispersion of hidden states and attention maps ($1 - \cos$), and (d) position-normalized generalized margin along the answer segment comparing driving and general data at $\tau \approx 1.0$.

informative layers, and we treat them as primary candidates.

Capability view. The representation view is insufficient to identify layers that encode stable, capability-level structure across images, so we further use capability-wise intra-consistency as a complementary criterion for layer selection. On the sampled dataset, for each layer ℓ and capability c , we compute an image–capability center by averaging the hidden vectors of the last non-special token over all questions of capability c for the same image:

$$\mathbf{c}_{c,\text{img}_g}^{(\ell)} = \frac{1}{N_{c,g}} \sum_{j=1}^{N_{c,g}} \mathbf{h}_{c,g,j}^{(\ell)}, \quad (4)$$

where $\mathbf{h}_{c,g,j}^{(\ell)}$ is the layer- ℓ hidden state of the last non-special token for the j -th question of capability c on image g . Let $\{\mathbf{c}_{c,\text{img}_1}^{(\ell)}, \dots, \mathbf{c}_{c,\text{img}_G}^{(\ell)}\}$ be the centers of capability c across G images; we define intra as the mean pairwise cosine similarity:

$$\text{intra}_c^{(\ell)} = \frac{2}{G(G-1)} \sum_{i < j} \cos(\mathbf{c}_{c,\text{img}_i}^{(\ell)}, \mathbf{c}_{c,\text{img}_j}^{(\ell)}), \quad (5)$$

where $\cos(\mathbf{a}, \mathbf{b}) = \langle \mathbf{a} / \|\mathbf{a}\|_2, \mathbf{b} / \|\mathbf{b}\|_2 \rangle$ and the summation is over all unordered image pairs ($i < j$).

Across all models, we observe consistent capability-specific patterns: perception has the highest intra at Layer 1 and then decreases with depth, reasoning keeps a high intra across layers, and planning decreases overall but shows a clear peak near Layer ℓ_{pen} ; together with the representation view, these results support selecting Layer 1 for perception, using broader intermediate layers for reasoning to connect early perception cues with later decision features, and using the penultimate layer for planning to leverage late-stage capability specialization while retaining upstream information.

3.2.2. WHAT TO DISTILL: SIGNAL SELECTION

For each (image, question) instance, we extract (i) the last non-special-token hidden vector and (ii) the head-mean at-

tention matrix at the target layer, and measure dispersion across questions for the same image using $1 - \cos(\cdot, \cdot)$, averaged over all question pairs and then over images.

For hidden states, for any two questions i and j paired under the same image, we compute the dispersion as $D_{\text{hid}}(i, j) = 1 - \cos(u_i, u_j)$, where u_i (resp. u_j) is the hidden vector at the target layer for the last token of the generated answer segment excluding special tokens.

For attention, we use the head-mean attention map \bar{A} and define $D_{\text{att}}(i, j) = 1 - \cos(\text{vec}(\tilde{A}_i), \text{vec}(\tilde{A}_j))$, where \tilde{A}_i and \tilde{A}_j are the overlap-aligned top-left submatrices of \bar{A}_i and \bar{A}_j with size $m = \min(L_i, L_j)$, corresponding to the shared prefix tokens (vision tokens + system prompt), and are flattened by $\text{vec}(\cdot)$ before cosine.

Across all three capabilities and all models, attention shows consistently lower dispersion than hidden states, indicating that attention reflects capability-stable behaviors more stably; therefore, we use attention as the distillation signal.

3.2.3. REVISITING OUTPUT-DISTRIBUTION ALIGNMENT

Output-distribution alignment is implemented as KL divergence between the teacher and student predictive distributions. However, its effectiveness is highly sensitive to teacher capability and task complexity. Across multiple temperatures, we feed the teacher model with both autonomous driving data and generic multimodal QA data, and quantify its confidence on answer tokens using top-1 probability, top-10 probability mass, and the generalized margin.

Let teacher logits at answer position t be $\mathbf{z}_t \in \mathbb{R}^{|\mathcal{V}|}$ and define the temperature-scaled softmax $p_t^{(\tau)}(k) = \text{softmax}(\mathbf{z}_t / \tau)_k$, we compute

$$m_t^{(\tau)} = \max_k p_t^{(\tau)}(k), \quad (6)$$

$$S_t^{(\tau)} = \sum_{i=1}^{10} p_t^{(\tau)}(k_i), \quad (7)$$

$$\Delta_{t,\text{gen}}^{(\tau)} = m_t^{(\tau)} - \frac{S_t^{(\tau)} - m_t^{(\tau)}}{10 - 1}. \quad (8)$$

where k_1, \dots, k_{10} index the top-10 tokens under $p_t^{(\tau)}$. The generalized margin $\Delta_{t,\text{gen}}^{(\tau)}$ measures the dominance of the top-1 token over the other top-10 candidates; larger values indicate higher confidence. Across all temperatures, driving outputs are consistently less confident and more diffuse than general outputs, making output-distribution alignment a noisy distillation signal; therefore, we do not include it as a distillation loss in Drive-KD.

3.3. Single-Teacher Distillation

3.3.1. DISTILLATION SIGNALS AND OBJECTIVES

We optimize the student with the hard-label supervised loss on our driving distillation dataset and add capability-specific attention distillation terms from a teacher.

Hard-label supervised loss. Given a token sequence $\{y_t\}_{t \in \mathcal{Y}_{\text{ans}}}$ over the answer span \mathcal{Y}_{ans} , the hard-label supervised loss is

$$L_{\text{sup}} = -\frac{1}{|\mathcal{Y}_{\text{ans}}|} \sum_{t \in \mathcal{Y}_{\text{ans}}} \log p_{\theta}(y_t \mid x, y_{<t}). \quad (9)$$

Attention Maps. Let $A_s^{(\ell)}, A_t^{(\ell)} \in \mathbb{R}^{B \times H \times L \times L}$ denote the attention weights at layer ℓ for the student and teacher. We first average attention over heads, where $(\cdot) \in \{s, t\}$:

$$\bar{A}_{(\cdot),b,i,j}^{(\ell)} = \frac{1}{H} \sum_{h=1}^H A_{(\cdot),b,h,i,j}^{(\ell)} \quad (10)$$

Full-attention distillation. We distill the full attention matrix by matching all query-to-key entries on valid positions between the student and teacher at layer ℓ , where i indexes the query token position and j indexes the key token position in a length- L sequence.

$$L_{\text{att}}^{\text{full}}(\ell) = \text{mean}_{b,i} \left[\text{mean}_j \left(\bar{A}_{s,b,i,j}^{(\ell)} - \bar{A}_{t,b,i,j}^{(\ell)} \right)^2 \right]. \quad (11)$$

We compute the squared error for each query-token (b, i) , average it over keys j , and then average over (b, i) .

Text-to-vision attention distillation. We compute the loss only over text query positions and normalize within each sample by the number of text-to-vision pairs. Let T_b and V_b denote the sets of text-query positions and vision-key positions in sample b , respectively, where T_b includes all text tokens in the prompt+answer sequence excluding special and padding tokens. The corresponding distillation loss is

$$L_{\text{att}}^{t-v}(\ell) = \text{mean}_b \frac{1}{|T_b| |V_b|} \sum_{i \in T_b} \sum_{j \in V_b} \left(\bar{A}_{s,b,i,j}^{(\ell)} - \bar{A}_{t,b,i,j}^{(\ell)} \right)^2. \quad (12)$$

We apply an online loss reweighting based on per-loss gradient magnitudes to stabilize multi-loss training. Further implementation details are provided in Appendix B.1. In this single-teacher stage, we do not use gradient projection, as it would dampen the attention-distillation gradients and thus confound a clean comparison among different distillation signals.

3.3.2. CAPABILITY-SPECIFIC RECIPES

We use hard-label supervision for all capabilities, and add capability-specific attention distillation as the soft term. For perception, we distill Layer 1 text-to-vision attention, $A_{1,t-v}$. For reasoning, we distill intermediate-layer attention with layer-group matching (Kim et al., 2025). Let the selected student layers be ℓ_1, \dots, ℓ_K and the selected teacher layers be k_1, \dots, k_M , where both sets are restricted to the range from Layer 1 to the penultimate layer ℓ_{pen} ; we set group size $g = \max(1, M - K + 1)$ and assign each student layer ℓ_i to a consecutive sliding teacher group $\mathcal{G}(\ell_i) = \{k_{s_i+1}, \dots, k_{s_i+g}\}$ with $s_i = \min(i - 1, M - g)$, using the mean attention over $\mathcal{G}(\ell_i)$ as the target. For planning, we distill penultimate-layer text-to-vision attention, $A_{\ell_{\text{pen}},t-v}$.

3.4. Multi-Teacher Distillation

3.4.1. OBJECTIVE AND TEACHER MIXING

Following the single-teacher recipes in Section 3.3.2, we define Drive-KD as a multi-teacher distillation framework with three teachers specialized for each capability, and we apply all three teachers to every batch. For a batch from capability c , we combine the three teachers with a fixed weight $\pi_{c,t}$, which sets how much teacher t contributes on capability c . Each teacher provides one capability-specific attention distillation loss L_t .

We use the following three definitions:

$$L_p = L_{\text{att}}^{t-v}(1). \quad (13)$$

$$L_r = \frac{1}{|\mathcal{S}|} \sum_{\ell \in \mathcal{S}} \text{mean}_{b,i} \left[\text{mean}_j \left(\bar{A}_{s,b,i,j}^{(\ell)} - \mu_{t,b,i,j}^{(\ell)} \right)^2 \right]. \quad (14)$$

$$\mu_{t,b,i,j}^{(\ell)} = \text{mean}_{k \in \mathcal{G}(\ell)} \bar{A}_{t,b,i,j}^{(k)}. \quad (15)$$

$$L_{pl} = L_{\text{att}}^{t-v}(\ell_{\text{pen}}), \quad \ell_{\text{pen}} = N_s - 1, \quad (16)$$

Here \mathcal{S} is the selected student layer set, and $\mathcal{G}(\ell)$ maps each $\ell \in \mathcal{S}$ to a small group of nearby teacher layers.

With these definitions, the total loss combines hard-label supervision with mixed distillation:

$$L = w_{\text{ce}} L_{\text{sup}} + \sum_{t \in \{p,r,pl\}} \pi_{c,t} w_t L_t. \quad (17)$$

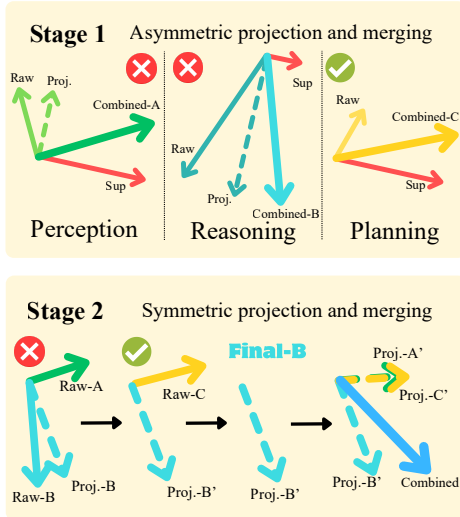


Figure 3. **Asymmetric Gradient Projection (AGP).** Stage 1 uses an asymmetric anchor–follower projection within each capability and merges the resulting update. Stage 2 applies shuffled symmetric pairwise projections across capabilities to obtain the final gradient direction (gradient B shown as an example).

3.4.2. ASYMMETRIC GRADIENT PROJECTION

To reduce gradient conflicts, we adopt AGP with two stages.

Stage 1: Asymmetric capability-wise projection and merging. For capability c , define $\mathbf{g}_{\text{sup}} = \nabla_{\theta}(w_{ce} L_{\text{sup}})$ and $\mathbf{g}_c = \nabla_{\theta}\left(\sum_{t \in \{p, r, pl\}} \pi_{c,t} w_t L_t\right)$; we use \mathbf{g}_{sup} as anchor and \mathbf{g}_c as follower.

$$\mathbf{g}_a^{(c)} = \mathbf{g}_{\text{sup}}, \quad \mathbf{g}_f = \mathbf{g}_c. \quad (18)$$

Then, we remove only the conflicting component of the follower along the anchor direction, while keeping the anchor unchanged:

$$\mathbf{g}_f \leftarrow \mathbf{g}_f - \frac{\mathbf{g}_f^\top \mathbf{g}_a^{(c)}}{\|\mathbf{g}_a^{(c)}\|_2^2} \mathbf{g}_a^{(c)}, \quad \text{if } \mathbf{g}_f^\top \mathbf{g}_a^{(c)} < 0 \quad (19)$$

We then merge the anchor and the follower to obtain the capability-level gradient used in Stage 2:

$$\mathbf{g}^{(c)} = \mathbf{g}_a^{(c)} + \mathbf{g}_f. \quad (20)$$

Stage 2: Symmetric pairwise projections among merged capability gradients. We have three capabilities $\mathcal{C} = \{p, r, pl\}$ and obtain merged gradients $\mathbf{g}^{(p)}, \mathbf{g}^{(r)}, \mathbf{g}^{(pl)}$ from Stage 1. To mitigate cross-capability conflicts, we check conflicts in a shuffled pairwise order and apply a projection only when a conflict is detected.

$$\tilde{\mathbf{g}}^{(c_1)} \leftarrow \mathbf{g}^{(c_1)}, \quad \tilde{\mathbf{g}}^{(c_2)} \leftarrow \mathbf{g}^{(c_2)}, \quad \tilde{\mathbf{g}}^{(c_3)} \leftarrow \mathbf{g}^{(c_3)}. \quad (21)$$

Specifically, we sample a random permutation (c_1, c_2, c_3) of (p, r, pl) and sequentially update each $\tilde{\mathbf{g}}^{(c_i)}$ by projecting it against the other two gradients in the order $c_1 \rightarrow c_2 \rightarrow c_3$.

$$\tilde{\mathbf{g}}^{(c_i)} \leftarrow \tilde{\mathbf{g}}^{(c_i)} - \frac{\tilde{\mathbf{g}}^{(c_i)\top} \mathbf{g}^{(c_j)}}{\|\mathbf{g}^{(c_j)}\|_2^2} \mathbf{g}^{(c_j)}, \quad \text{if } \tilde{\mathbf{g}}^{(c_i)\top} \mathbf{g}^{(c_j)} < 0 \quad (22)$$

Finally, we sum the projected capability gradients to form the overall update direction:

$$\mathbf{g} = \tilde{\mathbf{g}}^{(p)} + \tilde{\mathbf{g}}^{(r)} + \tilde{\mathbf{g}}^{(pl)}. \quad (23)$$

As shown in Figure 3, Stage 1 uses the hard-label supervised gradient as an anchor and removes only the part of the distillation update that conflicts with it, avoiding sacrificing hard-label learning to fit weaker teachers’ noisier or mismatched soft signals. Stage 2 resolves negative inner products among capability-level merged gradients to reduce the chance of improving one capability at the expense of another; the shuffled projection order further helps avoid consistently biasing toward any fixed capability.

4. Experiments

4.1. Experimental Setup

Data and prompts. We train on a 10k human-annotated driving distillation dataset with single-view and multi-view VQA; Appendix C.2 reports detailed diversity statistics, and Appendix C.3 provides annotated examples.

Models and training. Our main experiments consider two teacher-student pairs: InternVL3-8B → InternVL3-1B and Qwen2.5-VL-7B-Instruct → Qwen2.5-VL-3B-Instruct. We provide reproducibility details in Appendix D.1.

Evaluation. Evaluation is conducted on DriveBench (Xie et al., 2025). We merge DriveBench’s original prediction and behavior dimensions and report them jointly as reasoning. We use DeepSeek-V3.2 as the evaluator (Liu et al., 2025). We report capability scores for perception, reasoning, and planning, together with the overall average, and deployment-oriented inference metrics. Additional training and evaluation details, including evaluation-case illustrations, are provided in Appendix D.

4.2. Single-Teacher Evaluation

We evaluate single-teacher distillation by distilling each student from a single teacher within its model family. Each capability-specific single-teacher student is trained only on the corresponding capability split of our distillation dataset (Appendix C.2). In our setting, CE-only training is equivalent to SFT; we compare against this baseline in Section 4.5.

As summarized in Table 1, single-teacher distillation yields clear and consistent gains over pretrained baselines across

Table 1. Capability performance and deployment-oriented inference efficiency of representative VLMs on DriveBench. We report capability scores (%) and inference metrics, including peak GPU memory (GB) under the minimum viable number of GPUs, average GPU-side generation throughput (tokens/s), and median GPU-side time-to-first-token (s).

Model	Capability scores (%)				Deployment metrics		
	Perception	Reasoning	Planning	Avg.	Memory (GB)	Speed (tok/s)	1st-token (s)
GPT-5.1	45.56	41.02	51.94	46.17	-	-	-
InternVL3-1B	33.26	20.96	22.36	25.53	4.1	45.7	0.45
InternVL3-2B	37.71	35.99	26.19	33.30	6.3	39.9	0.67
InternVL3-8B	40.05	41.15	32.77	37.99	18.3	32.6	1.58
InternVL3-14B	39.83	40.84	36.35	39.01	33.4	17.0	3.01
InternVL3-38B	34.27	38.48	40.65	37.80	87.0	7.3	9.84
InternVL3-78B	42.01	47.16	36.31	41.83	171.6	4.0	16.46
Qwen2.5-VL-3B-Instruct	35.46	30.81	25.29	30.52	8.5	28.0	0.68
Qwen2.5-VL-7B-Instruct	36.26	37.54	32.84	35.55	17.1	32.0	0.87
Qwen2.5-VL-32B-Instruct	38.41	41.30	34.29	38.00	69.5	10.8	2.36
Qwen2.5-VL-72B-Instruct	23.78	27.67	50.76	34.07	146.5	5.8	4.26
Llama-3.2-11B-Vision-Instruct	31.59	32.91	29.34	31.28	26.2	16.8	1.55
Llama-3.2-90B-Vision-Instruct	27.26	26.33	27.72	27.10	183.6	2.7	8.05
InternVL3-1B (Single)	43.13	34.32	52.97	43.47	4.1	45.7	0.45
Qwen2.5-VL-3B-Instruct (Single)	45.59	34.47	51.97	44.01	8.5	28.0	0.68
InternVL3-1B (Multi)	43.50	33.15	55.51	44.05	4.1	45.7	0.45
Qwen2.5-VL-3B-Instruct (Multi)	45.63	36.41	54.07	45.37	8.5	28.0	0.68

both student families. Concretely, InternVL3-1B improves from 25.53 to 43.47 in Avg. score, and Qwen2.5-VL-3B-Instruct improves from 30.52 to 44.01. On planning, the distilled students become competitive with GPT-5.1: InternVL3-1B (Single) reaches 52.97 and Qwen2.5-VL-3B-Instruct (Single) reaches 51.97, compared with 51.94 for GPT-5.1. These results show that capability-focused internal-signal distillation can transfer driving-related behaviors to small students effectively.

Across these capabilities, the results follow a consistent trend. Perception improves strongly, matching our choice of early cross-modal attention for supervision. Reasoning also improves over pretrained baselines, but remains the hardest dimension: the gap to GPT-5.1 is larger than that in perception and planning, suggesting multi-step relation understanding is more difficult to transfer to a small VLM. Planning shows the largest gains and becomes the strongest dimension for distilled students, which supports our design of using late-stage cross-modal attention.

4.3. Multi-Teacher Evaluation

Compared with the single-teacher, multi-teacher training achieves a higher overall score (see Table 1). For InternVL3-1B, it improves Avg. from 43.47 to 44.05 and planning from 52.97 to 55.51, while preserving strong perception, highlighting the complementary benefits of Drive-KD.

By capability, perception stays on par with single-teacher, suggesting early-layer cross-modal supervision is already

sufficient. Reasoning remains comparable but appears most sensitive to cross-capability interference under multi-objective training. Planning improves the most and drives the higher average score, consistent with its reliance on integrating perception cues with intermediate reasoning signals, which multi-teacher supervision strengthens.

In terms of efficiency, the distilled models retain the lightweight deployment profile of small VLMs while achieving much stronger capability scores. For example, InternVL3-1B (Multi) uses 4.1 GB peak memory with 45.7 tok/s throughput, being far more efficient than pretrained InternVL3-78B (171.6 GB, 4.0 tok/s), yielding a substantially better capability-efficiency trade-off.

In the overall results (Table 1), GPT-5.1 scores higher on reasoning than the Drive-KD InternVL3-1B and Qwen2.5-VL-3B-Instruct student, but does not outperform them on planning. This motivates testing whether higher reasoning necessarily translates to better planning on the same visual inputs. For each image k , we average evaluator scores over its reasoning and planning questions to obtain R_k and P_k :

$$R_k = \text{mean}_{i \in \mathcal{Q}_r(k)} s_i, \quad P_k = \text{mean}_{j \in \mathcal{Q}_p(k)} s_j, \quad (24)$$

where s_i is the evaluator score for one (image, question) instance. We then compute Pearson and Spearman correlations between $\{R_k\}$ and $\{P_k\}$ over images that contain both question types. As shown in Table 2, GPT-5.1 shows near-zero reasoning–planning correlation, whereas our students exhibit a weak positive association. This suggests that Drive-KD not only improves planning scores, but also strengthens

Table 2. Image-level correlation between reasoning and planning scores.

Model	Pearson(R_k, P_k)	Spearman(R_k, P_k)
GPT-5.1	-0.0418	-0.0316
Ours (InternVL3)	+0.3384	+0.3724
Ours (Qwen2.5-VL)	+0.2976	+0.3271

Table 3. DriveBench scores (%) of InternVL3 students distilled from InternVL3 teachers. Here we abbreviate model size by parameter scale (e.g., 1B/2B/8B/14B/38B).

Tea	Stu	Perception	Reasoning	Planning	Avg.
8B	1B	43.50	33.15	55.51	44.05
14B	1B	43.41	30.34	56.19	43.31
38B	1B	43.24	29.15	56.77	43.05
8B	2B	43.14	36.97	56.01	45.37
14B	2B	41.74	35.40	56.84	44.66
38B	2B	42.87	38.25	57.63	46.25

same-scene reasoning–planning alignment, yielding a more consistent reasoning-to-planning mapping.

4.4. Distillation Scaling Across Model Sizes

We run the multi-teacher algorithm with teacher sizes {8B, 14B, 38B} and student sizes {1B, 2B}. Table 3 shows that for a fixed student, larger teachers can improve, match, or degrade different capabilities, and the best teacher size depends on student capacity. Meanwhile, under comparable distillation settings, the higher-capacity student is consistently stronger, indicating that student capacity remains crucial for absorbing transferred knowledge, and stronger teachers may be harder for small students to learn due to more complex feature representations. Overall, Drive-KD remains effective across different size pairings.

4.5. Ablation Study

We ablate six aspects on InternVL3-1B: (i) whether to add output-distribution alignment (CE+KL) beyond hard-label CE, (ii) hidden-state distillation variants, and (iii) gradient-conflict handling in multi-teacher training (none, G1/G2, or AGP). Here (i) and (ii) follow the single-teacher protocol: the model is trained on the corresponding capability split only, and we report the score on that capability (Table 4). The remaining three ablations are deferred to Appendix E, including alternative attention signals, similarity-based attention matching, and intermediate-layer range variants.

CE is equivalent to SFT, and KL aligns the output token distribution. “mid” denotes the intermediate layers from the first to the penultimate; G1 performs one joint symmetric projection across all losses, while G2 projects CE vs. soft within each capability and then projects across capabilities.

Table 4. InternVL3-1B ablations on DriveBench: distillation objectives and gradient-conflict handling.

Setting	Perception	Reasoning	Planning
CE	40.86	29.05	45.63
CE + KL	39.60	28.16	43.36
CE + Hidden (1)	41.27	-	-
CE + Hidden (mid)	-	31.65	-
CE + Hidden (ℓ_{pen})	-	-	45.04
Ours (single-teacher)	43.13	34.32	52.97
Multi-teacher	42.34	25.68	51.03
Multi-teacher (G1)	42.96	25.49	46.99
Multi-teacher (G2)	42.64	29.18	52.19
Ours (multi-teacher)	43.50	33.15	55.51

Overall, output-distribution alignment (KL) consistently degrades performance relative to CE, and comparisons against hidden-state distillation further support our signal choices; in contrast, our single-teacher recipe achieves the best overall performance. In multi-teacher training, the plain baseline severely hurts reasoning, and symmetric projection is also unstable—again most clearly on reasoning. A two-stage symmetric scheme (G2) recovers reasoning and improves planning, but AGP achieves the best planning score while keeping perception and reasoning strong. Together, these ablations support Drive-KD: capability-specific distillation signals and AGP are both critical for consistent gains.

5. Conclusion

We propose Drive-KD, a multi-teacher distillation framework for autonomous driving VLMs. Drive-KD decomposes driving into a sequential triad of perception, reasoning, and planning, and transfers each capability with targeted internal supervision. First, we present a systematic study of distillation design for driving VLMs. We identify Layer 1 cross-modal attention as most informative for perception, broader intermediate layers for reasoning, and the penultimate layer for planning. We find attention is more stable than hidden states, and output-distribution alignment is unreliable for autonomous driving. Second, based on these findings, we derive strong single-teacher recipes for each capability and improve small VLMs over baselines. Third, we unify the three capabilities into a multi-teacher framework and introduce AGP to reduce cross-capability interference. Finally, experiments show that distilled models achieve strong capability–efficiency trade-offs and Drive-KD generalizes across model scales and families. Our distilled InternVL3-1B uses $\sim 42 \times$ less peak GPU memory and achieves $\sim 11.4 \times$ higher generation throughput than pretrained InternVL3-78B, while outperforming it on DriveBench overall and surpassing GPT-5.1 on planning. We hope Drive-KD enables efficient driving VLMs and provides clearer insights into distilling capability-specific behaviors for safety-critical tasks.

Impact Statement

Drive-KD is expected to achieve faster on-vehicle response while improving driving capability. By lowering the hardware requirements for advanced AI safety functions, it may help make such functions available across a wider range of vehicle classes and price points. Compared with traditional end-to-end “black-box” models, our “perception–reasoning–planning” triad offers better interpretability. However, we acknowledge that reasoning ability remains the most difficult aspect to transfer to smaller models. Importantly, our results are based on the open-loop evaluation of DriveBench and do not guarantee real-world performance. We strongly recommend that any distilled model produced by Drive-KD undergo rigorous closed-loop simulation and extensive long-tail and edge-case testing before deployment in any physical system. For safety-critical deployment, potential risks should be assessed with particular caution.

References

Achiam, J., Adler, S., Agarwal, S., Ahmad, L., Akkaya, I., Aleman, F. L., Almeida, D., Altenschmidt, J., Altman, S., Anadkat, S., et al. Gpt-4 technical report. *arXiv preprint arXiv:2303.08774*, 2023.

Badue, C., Guidolini, R., Carneiro, R. V., Azevedo, P., Cardoso, V. B., Forechi, A., Jesus, L., Berriel, R., Paixao, T. M., Mutz, F., et al. Self-driving cars: A survey. *Expert systems with applications*, 165:113816, 2021.

Bai, J., Bai, S., Chu, Y., Cui, Z., Dang, K., Deng, X., Fan, Y., Ge, W., Han, Y., Huang, F., et al. Qwen technical report. *arXiv preprint arXiv:2309.16609*, 2023.

Bojarski, M., Del Testa, D., Dworakowski, D., Firner, B., Flepp, B., Goyal, P., Jackel, L. D., Monfort, M., Muller, U., Zhang, J., et al. End to end learning for self-driving cars. *arXiv preprint arXiv:1604.07316*, 2016.

Caesar, H., Bankiti, V., Lang, A. H., Vora, S., Lioung, V. E., Xu, Q., Krishnan, A., Pan, Y., Baldan, G., and Beijbom, O. nuscenes: A multimodal dataset for autonomous driving. In *Proceedings of the IEEE/CVF Conference on Computer Vision and Pattern Recognition (CVPR)*, June 2020.

Cao, J., Zhang, Y., Huang, T., Lu, M., Zhang, Q., An, R., Ma, N., and Zhang, S. MoVE-KD: Knowledge Distillation for VLMs with Mixture of Visual Encoders.

Chen, H., Quan, X., Chen, H., Yan, M., and Zhang, J. Knowledge distillation for closed-source language models. *arXiv preprint arXiv:2401.07013*, 2024a.

Chen, L., Wu, P., Chitta, K., Jaeger, B., Geiger, A., and Li, H. End-to-end autonomous driving: Challenges and frontiers. *IEEE Transactions on Pattern Analysis and Machine Intelligence*, 2024b.

Chen, Z., Wu, J., Wang, W., Su, W., Chen, G., Xing, S., Zhong, M., Zhang, Q., Zhu, X., Lu, L., et al. Internvl: Scaling up vision foundation models and aligning for generic visual-linguistic tasks. In *Proceedings of the IEEE/CVF Conference on Computer Vision and Pattern Recognition*, pp. 24185–24198, 2024c.

Feng, Q., Li, W., Lin, T., and Chen, X. Align-KD: Distilling Cross-Modal Alignment Knowledge for Mobile Vision-Language Model, December 2024. URL <http://arxiv.org/abs/2412.01282>. arXiv:2412.01282 [cs].

Gou, J., Yu, B., Maybank, S. J., and Tao, D. Knowledge distillation: A survey. *International journal of computer vision*, 129(6):1789–1819, 2021.

Gu, Y., Tong, Z., Castro, I., Wu, S., and Tyson, G. Multi-MLLM Knowledge Distillation for Out-of-Context News Detection, May 2025. URL <http://arxiv.org/abs/2505.22517>. arXiv:2505.22517 [cs].

Guan, T., Liu, F., Wu, X., Xian, R., Li, Z., Liu, X., Wang, X., Chen, L., Huang, F., Yacoob, Y., et al. Hallusionbench: an advanced diagnostic suite for entangled language hallucination and visual illusion in large vision-language models. In *Proceedings of the IEEE/CVF Conference on Computer Vision and Pattern Recognition*, pp. 14375–14385, 2024.

Guo, Z., Yagudin, Z., Lykov, A., Konenkov, M., and Tsetserukou, D. Vlm-auto: Vlm-based autonomous driving assistant with human-like behavior and understanding for complex road scenes. In *2024 2nd International Conference on Foundation and Large Language Models (FLLM)*, pp. 501–507. IEEE, 2024.

Hinton, G., Vinyals, O., and Dean, J. Distilling the knowledge in a neural network. *arXiv preprint arXiv:1503.02531*, 2015.

Hurst, A., Lerer, A., Goucher, A. P., Perelman, A., Ramesh, A., Clark, A., Ostrow, A., Welihinda, A., Hayes, A., Radford, A., et al. Gpt-4o system card. *arXiv preprint arXiv:2410.21276*, 2024.

Hwang, J.-J., Xu, R., Lin, H., Hung, W.-C., Ji, J., Choi, K., Huang, D., He, T., Covington, P., Sapp, B., Zhou, Y., Guo, J., Anguelov, D., and Tan, M. EMMA: End-to-End Multimodal Model for Autonomous Driving, September 2025. URL <http://arxiv.org/abs/2410.23262>. arXiv:2410.23262 [cs].

Kim, J., Kim, K., Seo, S., and Park, C. CompoDistill: Attention Distillation for Compositional Reasoning in Multimodal LLMs, October 2025. URL <http://arxiv.org/abs/2510.12184>. arXiv:2510.12184 [cs].

Li, P., Zhang, Z., Holtz, D., Yu, H., Yang, Y., Lai, Y., Song, R., Geiger, A., and Zell, A. Spacedrive: Infusing spatial awareness into vlm-based autonomous driving. *arXiv preprint arXiv:2512.10719*, 2, 2025a.

Li, X., Fang, Y., Liu, M., Ling, Z., Tu, Z., and Su, H. Distilling large vision-language model with out-of-distribution generalizability. In *Proceedings of the IEEE/CVF International Conference on Computer Vision*, pp. 2492–2503, 2023.

Li, Y., Yang, C., Dong, J., Yao, Z., Xu, H., Dong, Z., Zeng, H., An, Z., and Tian, Y. AMMKD: Adaptive Multimodal Multi-teacher Distillation for Lightweight Vision-Language Models, August 2025b. URL <http://arxiv.org/abs/2509.00039>. arXiv:2509.00039 [cs].

Li, Z., Wu, X., Du, H., Nghiem, H., and Shi, G. Benchmark evaluations, applications, and challenges of large vision language models: A survey. *arXiv preprint arXiv:2501.02189*, 1, 2025c.

Liang, C., Zuo, S., Zhang, Q., He, P., Chen, W., and Zhao, T. Less is more: Task-aware layer-wise distillation for language model compression. In *International Conference on Machine Learning*, pp. 20852–20867. PMLR, 2023.

Liu, A., Feng, B., Xue, B., Wang, B., Wu, B., Lu, C., Zhao, C., Deng, C., Zhang, C., Ruan, C., et al. Deepseek-v3 technical report. *arXiv preprint arXiv:2412.19437*, 2024.

Liu, A., Mei, A., Lin, B., Xue, B., Wang, B., Xu, B., Wu, B., Zhang, B., Lin, C., Dong, C., et al. Deepseek-v3. 2: Pushing the frontier of open large language models. *arXiv preprint arXiv:2512.02556*, 2025.

Lu, D., Sun, Y., Zhang, Z., Huang, L., Zeng, J., Shu, M., and Cao, H. Internvl-x: Advancing and accelerating internvl series with efficient visual token compression. *arXiv preprint arXiv:2503.21307*, 2025.

Mansourian, A. M., Ahmadi, R., Ghafouri, M., Babaie, A. M., Golezani, E. B., Ghamchi, Z. Y., Ramezanian, V., Taherian, A., Dinashi, K., Miri, A., et al. A comprehensive survey on knowledge distillation. *arXiv preprint arXiv:2503.12067*, 2025.

Moslemi, A., Briskina, A., Dang, Z., and Li, J. A survey on knowledge distillation: Recent advancements. *Machine Learning with Applications*, 18:100605, 2024.

Neo, C., Ong, L., Torr, P., Geva, M., Krueger, D., and Barez, F. Towards Interpreting Visual Information Processing in Vision-Language Models, April 2025. URL <http://arxiv.org/abs/2410.07149>. arXiv:2410.07149 [cs].

Paden, B., Čáp, M., Yong, S. Z., Yershov, D., and Frazzoli, E. A survey of motion planning and control techniques for self-driving urban vehicles. *IEEE Transactions on intelligent vehicles*, 1(1):33–55, 2016.

Pan, F., Zhang, Y., Liu, J., Head, L., Elli, M., and Alvarez, I. Reliability modeling for perception systems in autonomous vehicles: A recursive event-triggering point process approach. *Transportation Research Part C: Emerging Technologies*, 169:104868, 2024.

Pan, H., Wang, C., Qiu, M., Zhang, Y., Li, Y., and Huang, J. Meta-kd: A meta knowledge distillation framework for language model compression across domains. In *Proceedings of the 59th Annual Meeting of the Association for Computational Linguistics and the 11th International Joint Conference on Natural Language Processing (Volume 1: Long Papers)*, pp. 3026–3036, 2021.

Pham, C., Hoang, T., and Do, T.-T. Collaborative multi-teacher knowledge distillation for learning low bit-width deep neural networks. In *Proceedings of the IEEE/CVF Winter Conference on Applications of Computer Vision (WACV)*, pp. 6435–6443, January 2023.

Shao, H., Hu, Y., Wang, L., Song, G., Waslander, S. L., Liu, Y., and Li, H. LMDrive: Closed-Loop End-to-End Driving with Large Language Models. In *2024 IEEE/CVF Conference on Computer Vision and Pattern Recognition (CVPR)*, pp. 15120–15130, Seattle, WA, USA, June 2024. IEEE. ISBN 979-8-3503-5300-6. doi: 10.1109/CVPR52733.2024.01432. URL <https://ieeexplore.ieee.org/document/10657019/>.

Sima, C., Renz, K., Chitta, K., Chen, L., Zhang, H., Xie, C., Beißenwenger, J., Luo, P., Geiger, A., and Li, H. DriveLM: Driving with Graph Visual Question Answering, January 2025. URL <http://arxiv.org/abs/2312.14150>. arXiv:2312.14150 [cs].

Tampuu, A., Matiisen, T., Semikin, M., Fishman, D., and Muhammad, N. A survey of end-to-end driving: Architectures and training methods. *IEEE Transactions on Neural Networks and Learning Systems*, 33(4):1364–1384, 2020.

Tang, Z., Wang, Z., Wang, Y., Lian, W., Gao, T., Li, H., Ru, T., Meng, L., Cui, Z., Zhu, Y., et al. Autodridm: An explainable benchmark for decision-making of vision-language models in autonomous driving. *arXiv preprint arXiv:2601.14702*, 2026.

Team, Q. Qwen2.5-vl, January 2025. URL <https://qwenlm.github.io/blog/qwen2.5-vl/>.

Tian, H., Xu, B., Li, S., and Jin, X. From Low-Rank Features to Encoding Mismatch: Rethinking Feature Distillation in Vision Transformers, November 2025. URL <http://arxiv.org/abs/2511.15572>. arXiv:2511.15572 [cs].

Tian, X., Gu, J., Li, B., Liu, Y., Wang, Y., Zhao, Z., Zhan, K., Jia, P., Lang, X., and Zhao, H. DriveVLM: The Convergence of Autonomous Driving and Large Vision-Language Models, June 2024. URL <http://arxiv.org/abs/2402.12289>. arXiv:2402.12289 [cs].

Vougioukas, S. G. Agricultural robotics. *Annual review of control, robotics, and autonomous systems*, 2(1):365–392, 2019.

Wang, J., Liao, D., Zhang, Y., Xu, D., and Zhang, X. Layerwised multimodal knowledge distillation for vision-language pretrained model. *Neural Networks*, 175:106272, 2024a.

Wang, P., Bai, S., Tan, S., Wang, S., Fan, Z., Bai, J., Chen, K., Liu, X., Wang, J., Ge, W., et al. Qwen2-vl: Enhancing vision-language model’s perception of the world at any resolution. *arXiv preprint arXiv:2409.12191*, 2024b.

Xie, S., Kong, L., Dong, Y., Sima, C., Zhang, W., Chen, Q. A., Liu, Z., and Pan, L. Are vlms ready for autonomous driving? an empirical study from the reliability, data and metric perspectives. In *Proceedings of the IEEE/CVF International Conference on Computer Vision (ICCV)*, pp. 6585–6597, October 2025.

Xu, X., Li, M., Tao, C., Shen, T., Cheng, R., Li, J., Xu, C., Tao, D., and Zhou, T. A survey on knowledge distillation of large language models. *arXiv preprint arXiv:2402.13116*, 2024a.

Xu, X., Li, M., Tao, C., Shen, T., Cheng, R., Li, J., Xu, C., Tao, D., and Zhou, T. A Survey on Knowledge Distillation of Large Language Models, October 2024b. URL <http://arxiv.org/abs/2402.13116>. arXiv:2402.13116 [cs].

Xu, Z., Bai, Y., Zhang, Y., Li, Z., Xia, F., Wong, K.-Y. K., Wang, J., and Zhao, H. DriveGPT4-V2: Harnessing Large Language Model Capabilities for Enhanced Closed-Loop Autonomous Driving.

Xu, Z., Zhang, Y., Xie, E., Zhao, Z., Guo, Y., Wong, K.-Y. K., Li, Z., and Zhao, H. DriveGPT4: Interpretable End-to-end Autonomous Driving via Large Language Model, November 2024c. URL <http://arxiv.org/abs/2310.01412>. arXiv:2310.01412 [cs].

Yang, X., Lu, J., and Yu, E. Learning from All: Concept Alignment for Autonomous Distillation from Multiple Drifting MLLMs, October 2025. URL <http://arxiv.org/abs/2510.04142>. arXiv:2510.04142 [cs].

You, J., Jiang, Z., Huang, Z., Shi, H., Gan, R., Wu, K., Cheng, X., Li, X., and Ran, B. V2x-vlm: End-to-end v2x cooperative autonomous driving through large vision-language models. *Transportation Research Part C: Emerging Technologies*, 183:105457, 2026.

Yu, F., Chen, H., Wang, X., Xian, W., Chen, Y., Liu, F., Madhavan, V., and Darrell, T. Bdd100k: A diverse driving dataset for heterogeneous multitask learning. In *IEEE/CVF Conference on Computer Vision and Pattern Recognition (CVPR)*, June 2020.

Yurtsever, E., Lambert, J., Carballo, A., and Takeda, K. A survey of autonomous driving: Common practices and emerging technologies. *IEEE access*, 8:58443–58469, 2020.

Zhang, H., Chen, D., and Wang, C. Adaptive multi-teacher knowledge distillation with meta-learning, 2023.

Zhang, J., Huang, J., Jin, S., and Lu, S. Vision-language models for vision tasks: A survey. *IEEE transactions on pattern analysis and machine intelligence*, 46(8):5625–5644, 2024.

Zhao, J., Zhao, W., Deng, B., Wang, Z., Zhang, F., Zheng, W., Cao, W., Nan, J., Lian, Y., and Burke, A. F. Autonomous driving system: A comprehensive survey. *Expert Systems with Applications*, 242:122836, 2024. ISSN 0957-4174. doi: <https://doi.org/10.1016/j.eswa.2023.122836>. URL <https://www.sciencedirect.com/science/article/pii/S0957417423033389>.

Zhao, W. X., Zhou, K., Li, J., Tang, T., Wang, X., Hou, Y., Min, Y., Zhang, B., Zhang, J., Dong, Z., et al. A survey of large language models. *arXiv preprint arXiv:2303.18223*, 1(2), 2023.

Zhong, Q., Ding, L., Shen, L., Liu, J., Du, B., and Tao, D. Revisiting Knowledge Distillation for Autoregressive Language Models, June 2024. URL <http://arxiv.org/abs/2402.11890>. arXiv:2402.11890 [cs].

Zhou, X., Liu, M., Yurtsever, E., Zagar, B. L., Zimmer, W., Cao, H., and Knoll, A. C. Vision language models in autonomous driving: A survey and outlook. *IEEE Transactions on Intelligent Vehicles*, 2024.

Zhu, Y., Zhu, M., Liu, N., Xu, Z., and Peng, Y. Llava-phi: Efficient multi-modal assistant with small language model. In *Proceedings of the 1st International Workshop on Efficient Multimedia Computing under Limited*, pp. 18–22, 2024.

A. Additional Pre-study Analyses

A.1. Layer-wise similarity profiles across model families and scales

We report additional layer-wise similarity profiles (Figure 4) to support our layer selection criteria across model families and parameter scales.

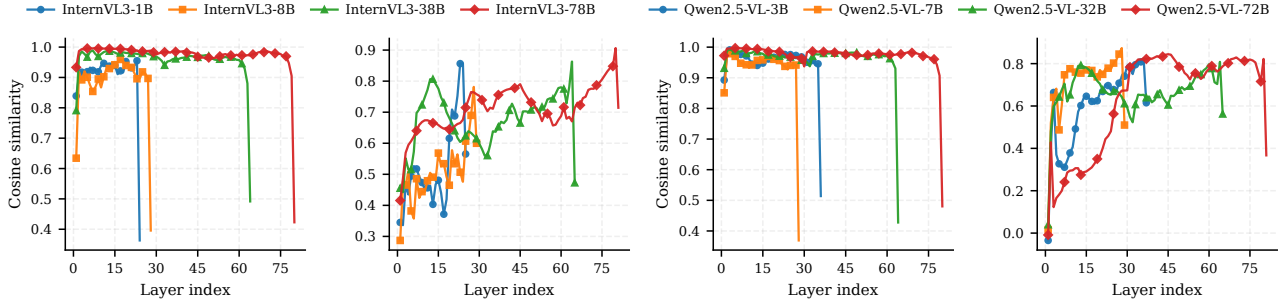


Figure 4. Layer-wise similarity profiles across model families and scales. Adjacent-layer cosine similarity (Adj. CosSim) and within-layer vision–text cosine similarity (V–T CosSim) are shown for InternVL3 (1B/8B/38B/78B) and Qwen2.5-VL (3B/7B/32B/72B).

A.2. Capability-wise intra-consistency across Transformer layers

We further include capability-wise intra-consistency curves (Figure 5), which complement representation-based signals by quantifying how stable each capability representation is across images at different depths.

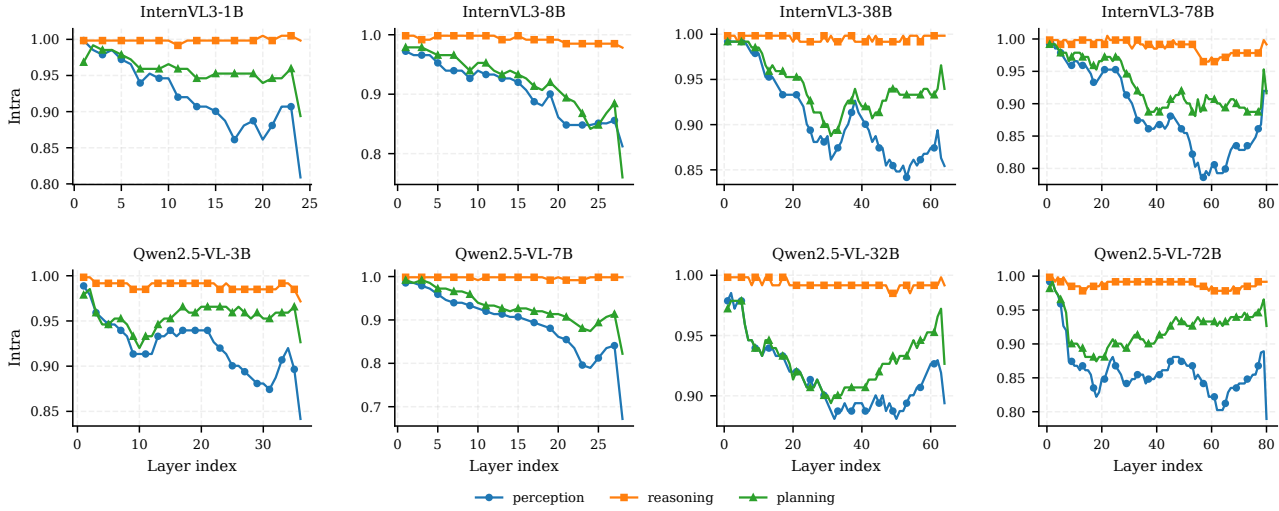


Figure 5. Capability-wise intra-consistency (mean pairwise cosine similarity) across Transformer layers for InternVL3 (top row) and Qwen2.5-VL (bottom row) under three task types: perception, reasoning, and planning.

A.3. Hidden-state vs. attention dispersion under rewording

We provide dispersion comparisons between hidden states and attention maps under question rewording (Figure 6) to justify using attention as a more capability-stable distillation signal.

A.4. Position-wise output-distribution alignment analyses

We present position-wise analyses for output-distribution alignment under multiple temperatures (Figures 7 and 8), contrasting driving and general answers to clarify why KL-based output alignment can become noisy on driving outputs.

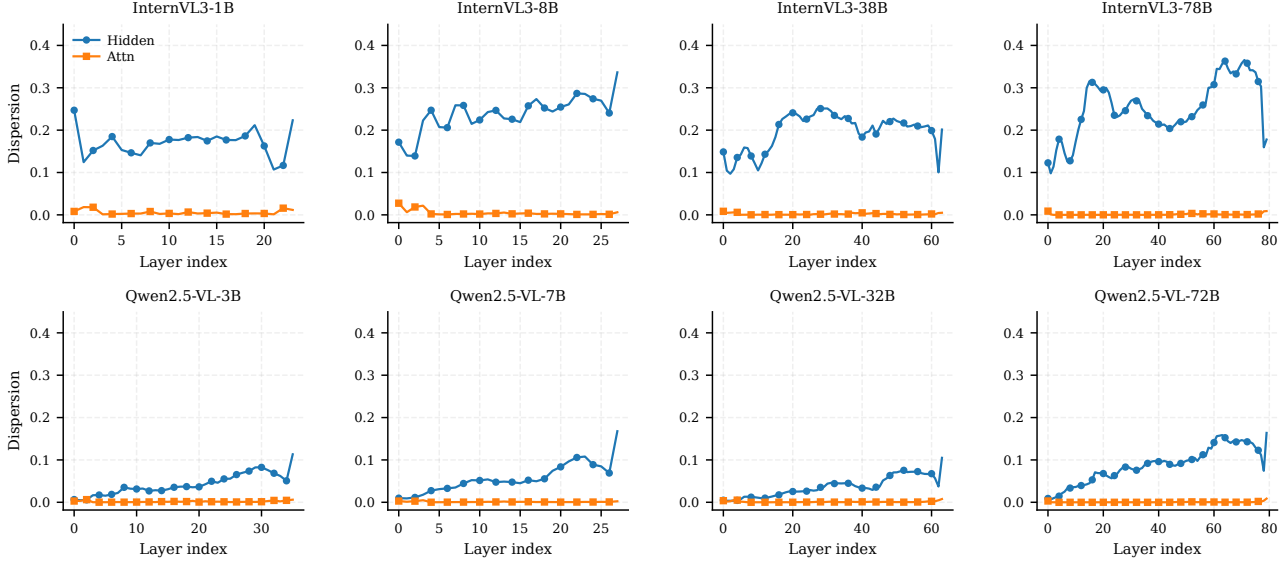


Figure 6. Hidden-state vs. attention dispersion under rewording for InternVL3 and Qwen2.5-VL model families. Each subplot corresponds to one model; the x-axis is the Transformer layer index and the y-axis is dispersion measured as $1 - \cos(\cdot, \cdot)$ on the all-capabilities aggregate. We report dispersion curves for the last-token hidden representation (Hidden) and the head-mean attention map (Attn). Lower values indicate more stable signals across different question rephrasings on the same image.

B. Optimization Details

This section details the online loss reweighting procedure used in training, including how per-loss gradient magnitudes are estimated and how the weights are updated to stabilize multi-objective optimization.

B.1. Online loss reweighting strategy.

We use an online loss reweighting strategy to stabilize multi-objective training, balancing the influence of different losses on parameter updates and reducing sensitivity to manual tuning. Specifically, each loss term L_i is assigned a positive learnable weight w_i , and we jointly optimize the weighted sum $\sum_i w_i L_i$ together with the student model. At each optimization step, we estimate the gradient magnitude of each loss as $G_i = \|\nabla_{\theta} L_i\|_2$ and update $\{w_i\}$ so that the weighted magnitudes $w_i G_i$ approach a target value. The target combines a preset static weight ratio p_i and the relative decay rate of each loss, where s indexes training steps:

$$\hat{G}_i \propto p_i \left(\frac{L_i(s)/L_i(0)}{\frac{1}{N} \sum_{j \in \mathcal{I}} L_j(s)/L_j(0)} \right)^{\alpha}. \quad (25)$$

We encourage the weighted gradient strengths to satisfy $w_i G_i \approx \hat{G}_i$. Here \mathcal{I} is the set of active loss terms and $N = |\mathcal{I}|$, while α controls how strongly the reweighting reacts to relative loss decay.

C. Annotated Distillation Data

C.1. Dataset Sources and Annotation Format

Multi-view image groups are sampled from nuScenes, and single-view images are sampled from both nuScenes and BDD100K (Caesar et al., 2020; Yu et al., 2020). For each image (single-view) or image group (multi-view), we annotate eight driving-related question types spanning the sequential triad of perception, reasoning, and planning. Each instance is paired with a human reference answer consisting of a brief final response and a detailed chain-of-thought rationale.

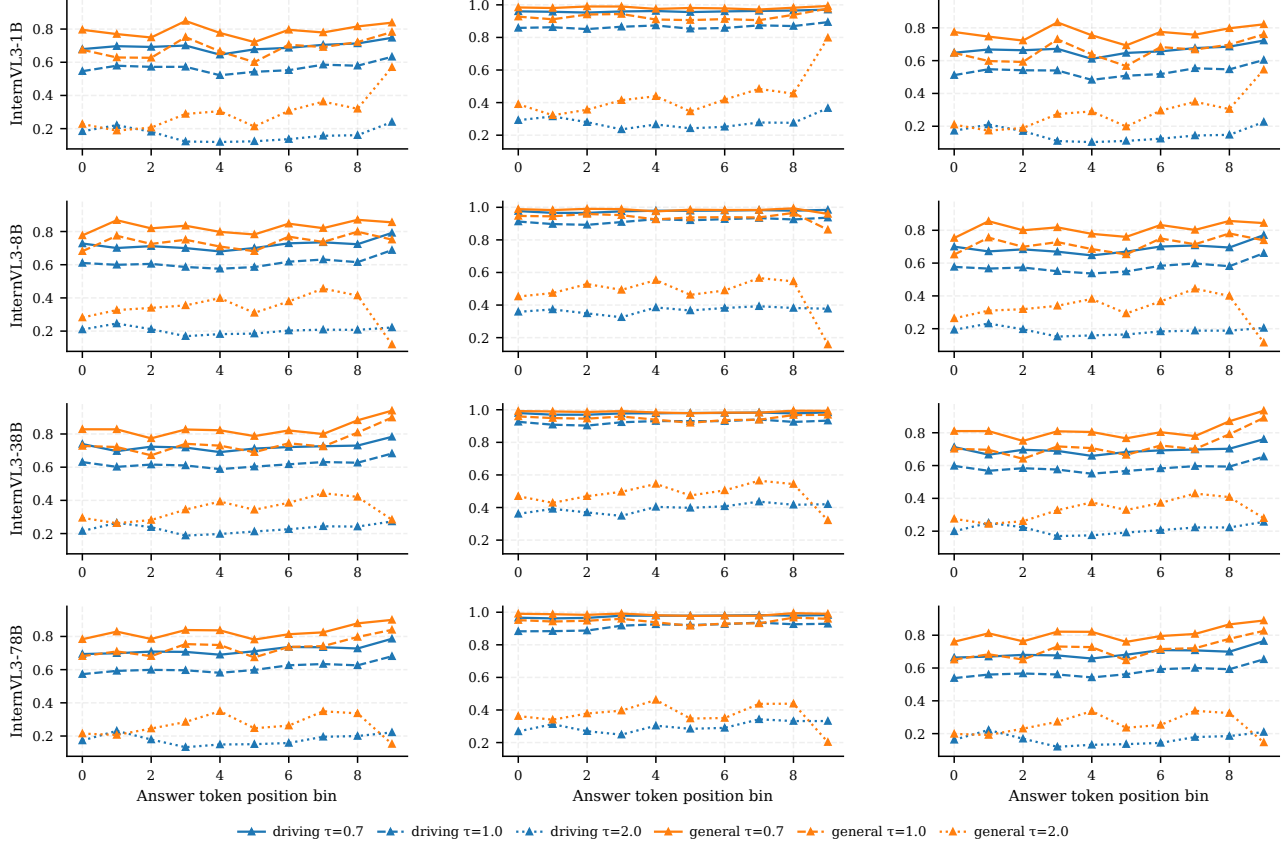


Figure 7. Output-distribution alignment (KL) analysis on answer-token position bins for the InternVL3 family. Rows correspond to models (1B/8B/38B/78B), and columns report three confidence metrics: top-1 probability m , top-10 mass S , and generalized margin. For each subplot, we compare *driving* vs. *general* answers under three temperatures ($\tau \in \{0.7, 1.0, 2.0\}$), using consistent colors (split) and line styles (temperature).

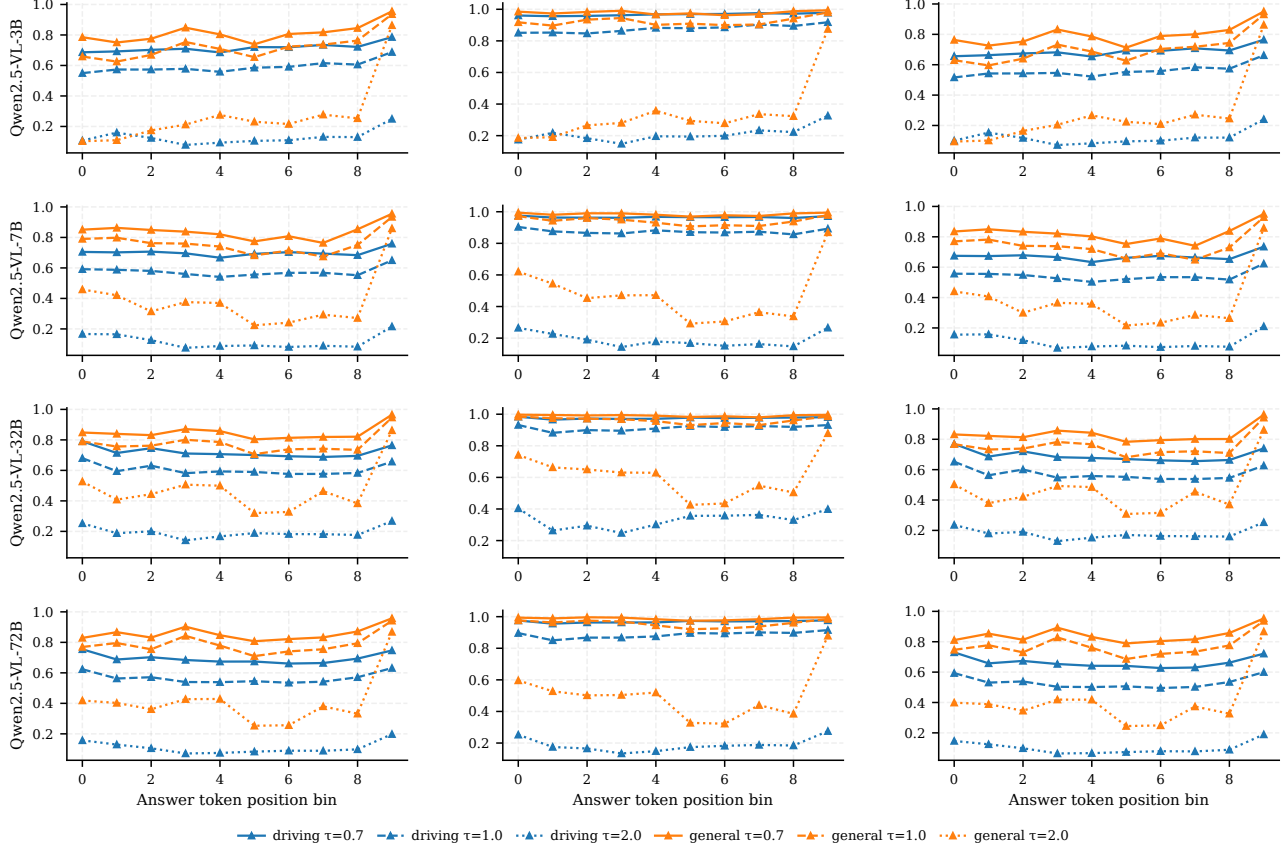


Figure 8. KL-based logit distillation analyses on answer-token position bins for the Qwen2.5-VL family. Rows correspond to models (3B/7B/32B/72B), and columns report three confidence metrics: top-1 probability m , top-10 mass S , and generalized margin. Each subplot contrasts *driving* vs. *general* answers under three temperatures ($\tau \in \{0.7, 1.0, 2.0\}$), with consistent colors (split) and line styles (temperature).

C.2. Dataset Diversity Statistics

Our human annotations span eight driving-related question types, including motion status, target identification, multi-view object extraction and attention-based reasoning, ego-behavior reasoning, rationale-grounded planning decisions, safe-action set analysis, and collision-inducing action analysis. The dataset spans three capability categories, and includes both single-image and six-image settings (56.23% vs. 43.77%), where the latter covers surround-view camera perspectives. In addition, targets are broadly distributed in the image space: center-mid 43.10%, right-mid 13.95%, left-mid 11.85%, center-bottom 10.57%, right-bottom 7.41%, left-bottom 4.84%, center-top 4.45%, right-top 2.46%, and left-top 1.37%.

At the object level, for road-structure and traffic-rule related objects, lane accounts for 59.60%, traffic sign 25.90%, and traffic light/traffic signal 9.97%, along with long-tail elements such as crosswalk, curb, sidewalk, and stop sign. For vehicles, sedan accounts for 43.35%, SUV 26.96%, and truck/van 21.40%, and the annotations also include bus, pickup, and taxi. For vulnerable road users, the annotations cover pedestrians, motorcycles, bicycles, and cyclists. These objects are accompanied by precise color and shape descriptions.

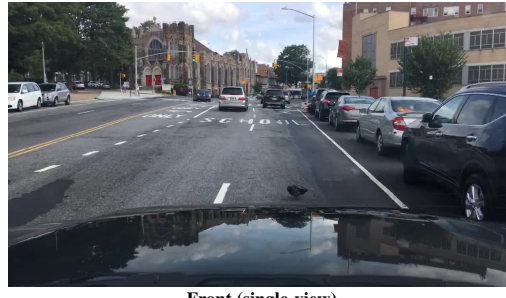
At the scene level, the annotations span diverse road structures and interactions, dominated by turning (50.20%) and intersections (14.21%), followed by lane change (8.74%), parking (8.55%), and crosswalk areas (7.19%), with additional coverage of construction, traffic jams and ramp merges. Weather and time-of-day mentions are also diverse (clear/rain/overcast, plus snow/wind/fog; and night/daytime/dawn–dusk). The action space includes both routine safe decisions and counterfactual risky behaviors: stop (26.69%), keep speed (15.98%), turn right/left (14.63%/14.15%), gentle braking to stop (7.75%), gradual deceleration without braking (4.83%), slight offset left/right (6.53% total), lane change left/right (3.34% total), and collision-oriented counterfactuals such as accelerating straight (3.40%) as well as sustained deviation and sharp turns.

Finally, at the language level, the average annotation length is about 61 words / 410 characters, with a clear spread (p25=48 words, p75=71 words, max=205 words), demonstrating rich variation in expression and explanatory details.

C.3. Annotated examples

We group representative annotated examples for perception, reasoning, and planning (Figures 9 to 11) to illustrate the format of our 10k distillation dataset. Each instance contains a brief answer to the question followed by a detailed chain-of-thought rationale.

Annotated Example (Perception)



Front (single-view)

Question: What is the moving status of object <c1,CAM_FRONT,0.3843,0.3338>? Please select the correct answer from the following options:

A. Going ahead. B. Turn left. C. Turn right.

Answer: B

Rationale: Objects: Black SUV (ID 1). Location & orientation: left of ego at mid-distance; its heading shows a slight tilt to the left, indicating a left turn relative to the lane/curb. Environment: cloudy weather, dry road surface, green traffic signal. Reasoning: the observed trajectory and slight leftward tilt, together with its position in the left lane, indicate it is turning left; lane markings and alignment with the curb further support this motion state.

Figure 9. Perception annotation example from our 10k distillation dataset.

Annotated Example (Reasoning)



Question: Predict the behavior of the ego vehicle. Please select the correct answer from the following options: A. The ego vehicle is slightly steering to the right, driving with normal speed. B. ... C. ... D. ...

Answer: A

Rationale: The vehicle is traveling at the intersection of two straight roads. Object <own vehicle> is located in the middle of the road, facing directly forward relative to the camera. Based on the road markings and the vehicle's orientation in the scene, its behavior is judged as **A**. The weather is clear, which does not alter the judgment.

Figure 10. Reasoning annotation example from our 10k distillation dataset.

Annotated Example (Planning)



Question: In this scenario, what are safe actions to take for the ego vehicle?

Answer: keep going at the same speed; decelerate gradually without braking

Rationale: The road ahead is clear with no immediate obstacles or traffic, and the lane markings indicate a straight path. The presence of a bus in the distance suggests normal traffic flow, so maintaining speed or gently reducing it is appropriate.

Figure 11. Planning annotation example from our 10k distillation dataset.

D. Training and Evaluation Details

D.1. Reproducibility details.

To facilitate reproducibility, we report the full training configuration used in all main distillation experiments. **Training setup.** We use full-parameter fine-tuning with a fixed random seed of 42 on NVIDIA A100-PCIE-40GB GPUs. We train for 3 epochs on our 10k human-annotated driving distillation dataset.

Optimization hyperparameters. The student model is optimized with AdamW. We use a learning rate of 5×10^{-5} . We set gradient accumulation steps to 4. We use a cosine learning-rate scheduler with a warmup ratio of 0.03 and a minimum learning-rate ratio of 0.01. We set the micro-batch size to 1, and use gradient accumulation with 4 steps, resulting in an effective batch size of $1 \times 4 = 4$.

Online loss reweighting implementation. In Appendix B.1, we parameterize each learnable loss weight as $w_i = \text{softplus}(a_i) + \epsilon$ with $\epsilon = 10^{-8}$. We then apply a bounded constraint to w_i and use small positive epsilons for numerical stability. The dynamic-weight parameters $\{a_i\}$ are optimized with AdamW using learning rate 3×10^{-4} , with standard numerical-stability safeguards. We additionally apply a bounded constraint to the learned dynamic weights to avoid extreme values during training.

AGP numerical stability. In the projection operator in Appendix 3.4.2, we add a small denominator constant $\epsilon_{\text{proj}} = 10^{-20}$ when computing $\|g\|_2^2$. This prevents division-by-zero in degenerate cases.

Teacher mixing weights. In multi-teacher training (Appendix 3.4.1), for a batch from capability $c \in \{p, r, pl\}$, we use the fixed teacher-mixing matrix

$$\Pi = \begin{bmatrix} 0.8 & 0.1 & 0.1 \\ 0.1 & 0.8 & 0.1 \\ 0.1 & 0.1 & 0.8 \end{bmatrix}. \quad (26)$$

Each capability is biased toward its specialized teacher while keeping non-zero contributions from the other teachers. This reduces overfitting to a single capability and mitigates catastrophic forgetting across capabilities.

Code release. We plan to release our code (training, distillation, and evaluation scripts) after publication.

D.2. Inference metrics.

Peak GPU memory (GB). We run inference with the minimum number of GPUs that can successfully execute the model, and report peak GPU memory as the maximum total memory usage summed over all GPUs observed during the run.

Average generation throughput (tokens/s). Average generation throughput is defined as the number of newly generated tokens divided by the total generation time:

$$\text{avg_gen_tokens_per_s} = \frac{\text{total_gen_tokens}}{\text{gen_time_total_s}}, \quad (27)$$

where `total_gen_tokens` excludes input prompt tokens.

Median TTFT (seconds). We measure TTFT by repeatedly running generation with `max_new_tokens = 1` and recording the elapsed time to produce the first token. We report the median over runs:

$$\text{ttft_s_median} = \text{median}(\{T_i\}). \quad (28)$$

D.3. LLM-based grading protocol.

DriveBench uses an LLM-based grader with predefined rules and scene metadata. In our evaluation, we keep the grading prompt fixed and run grading five times, reporting the average score to reduce randomness. We quantify the stochasticity of LLM-based grading by reporting the run-to-run standard deviation of the aggregated capability scores over the five independent grading runs. Specifically, for each model and capability, let $\{s_i\}_{i=1}^5$ be the overall DriveBench score (%) from

the i -th grading run and $\bar{s} = \frac{1}{5} \sum_{i=1}^5 s_i$ be the mean. We report the sample standard deviation

$$\sigma = \sqrt{\frac{1}{5-1} \sum_{i=1}^5 (s_i - \bar{s})^2}. \quad (29)$$

Table 5 lists σ for all models in Table 1.

Table 5. Run-to-run standard deviation σ (%) of DriveBench capability scores over five DeepSeek-V3.2 grading runs for the models in Table 1.

Model	Perception σ	Reasoning σ	Planning σ
GPT-5.1	1.1787	1.5382	1.4031
InternVL3-1B	0.9494	1.9117	1.6508
InternVL3-2B	1.3180	1.5707	1.4936
InternVL3-8B	0.8428	1.6398	1.5451
InternVL3-14B	0.8410	1.6294	1.6342
InternVL3-38B	1.1267	1.6408	1.5969
InternVL3-78B	1.2724	1.5285	1.7304
Qwen2.5-VL-3B-Instruct	1.2111	1.7037	1.3293
Qwen2.5-VL-7B-Instruct	1.3538	1.7018	1.2906
Qwen2.5-VL-32B-Instruct	0.8797	1.9699	1.6058
Qwen2.5-VL-72B-Instruct	1.2711	1.9081	1.5641
Llama-3.2-11B-Vision-Instruct	1.3626	1.7238	1.5739
Llama-3.2-90B-Vision-Instruct	1.2834	1.8497	1.7649
InternVL3-1B (Single)	1.1445	1.8949	1.2617
Qwen2.5-VL-3B-Instruct (Single)	0.9520	1.6770	1.2826
InternVL3-1B (Multi)	0.9547	1.5781	1.4049
Qwen2.5-VL-3B-Instruct (Multi)	1.1767	1.7166	1.4617

D.4. Evaluation-case illustration.

We provide concrete evaluation-case illustrations, clarifying how our protocol is applied in practice. Specifically, Figures 12 to 14 present representative cases for perception, reasoning, and planning, respectively.

E. Additional Attention Distillation Variants

This appendix reports supplementary ablation results. We compare three types of variants against our final single-teacher recipe. First, we test alternative attention targets that deviate from our recipe: using full attention at Layer 1 for perception, using text-to-vision attention (A_{t-v}) in intermediate layers for reasoning, and using full attention at ℓ_{pen} for planning. Second, for reasoning, we change the intermediate-layer distillation range to avoid overlap with the perception/planning layers, using Layer 2 to Layer $\ell_{\text{pen}} - 1$ (i.e., the second layer to the third-from-last layer). Third, we test similarity-based loss as a replacement for MSE. We consider two attention targets: (i) full attention, which matches all query–key entries of the head-mean attention matrix, and (ii) text-to-vision attention A_{t-v} , which matches the submatrix whose queries are text tokens and keys are vision tokens. In all attention-based distillation losses, we apply the standard attention masks (causal and padding) and compute the objective only on valid query–key positions shared by the teacher and student sequences. For A_{t-v} , we define T_b as the set of all text-query token positions in the concatenated prompt+answer sequence (excluding special and padded tokens), and define V_b as the set of all vision-key token positions. In the reasoning range variant, “mid (2 → $\ell_{\text{pen}} - 1$)” denotes Layer 2 to Layer $\ell_{\text{pen}} - 1$. For similarity-based loss, we define cosine-based attention matching as a replacement for MSE.

Perception / planning (single-layer A_{t-v} cosine loss). We apply a cosine-based loss to the text-to-vision attention A_{t-v} at Layer 1 and ℓ_{pen} , respectively. For sample b , let T_b be the index set of text-query positions and V_b be the index set of vision-key positions. Define the vectorization operator $\text{vec}_{t-v}(\bar{A}_{(\cdot),b}^{(\ell)}) \in \mathbb{R}^{|T_b||V_b|}$ that stacks the entries $\{\bar{A}_{(\cdot),b,i,j}^{(\ell)}\}_{i \in T_b, j \in V_b}$.

We then apply L_2 normalization and compute cosine dissimilarity:

$$\tilde{\mathbf{a}}_{(\cdot),b,t-v}^{(\ell)} = \text{vec}_{t-v} \left(\bar{A}_{(\cdot),b}^{(\ell)} \right), \quad \hat{\mathbf{a}}_{(\cdot),b,t-v}^{(\ell)} = \frac{\tilde{\mathbf{a}}_{(\cdot),b,t-v}^{(\ell)}}{\left\| \tilde{\mathbf{a}}_{(\cdot),b,t-v}^{(\ell)} \right\|_2 + \epsilon}, \quad (30)$$

where ϵ is a small constant for numerical stability. The cosine loss is

$$\mathcal{L}_{\text{att}}^{\text{sim-}t-v}(\ell) = \text{mean}_b \left[1 - \cos \left(\hat{\mathbf{a}}_{s,b,t-v}^{(\ell)}, \hat{\mathbf{a}}_{t,b,t-v}^{(\ell)} \right) \right], \quad (31)$$

where $\cos(\mathbf{u}, \mathbf{v}) = \mathbf{u}^\top \mathbf{v}$ for L_2 -normalized vectors.

Reasoning (grouped intermediate layers; full-attention cosine loss). For intermediate-layer reasoning supervision, teacher and student may have different depths. We therefore reuse the layer-group matching in Section 3.3.2: let the selected student layer set be \mathcal{S} and map each $\ell \in \mathcal{S}$ to a nearby teacher-layer group $\mathcal{G}(\ell)$. We form the teacher target as the group-mean head-mean attention:

$$\mu_{t,b,i,j}^{(\ell)} = \text{mean}_{k \in \mathcal{G}(\ell)} \bar{A}_{t,b,i,j}^{(k)}. \quad (32)$$

Let $\text{vecfull}(\cdot)$ stack all entries of a head-mean full attention matrix. We define the student/teacher attention vectors and apply L_2 normalization:

$$\tilde{\mathbf{a}}_{s,b,\text{full}}^{(\ell)} = \text{vecfull} \left(\bar{A}_{s,b}^{(\ell)} \right), \quad \tilde{\mathbf{a}}_{t,b,\text{full}}^{(\ell)} = \text{vecfull} \left(\mu_{t,b}^{(\ell)} \right), \quad (33)$$

$$\hat{\mathbf{a}}_{(\cdot),b,\text{full}}^{(\ell)} = \frac{\tilde{\mathbf{a}}_{(\cdot),b,\text{full}}^{(\ell)}}{\left\| \tilde{\mathbf{a}}_{(\cdot),b,\text{full}}^{(\ell)} \right\|_2 + \epsilon}. \quad (34)$$

The grouped cosine distillation loss is

$$\mathcal{L}_{\text{att}}^{\text{sim-full}} = \text{mean}_b \left[\frac{1}{|\mathcal{S}|} \sum_{\ell \in \mathcal{S}} \left(1 - \cos \left(\hat{\mathbf{a}}_{s,b,\text{full}}^{(\ell)}, \hat{\mathbf{a}}_{t,b,\text{full}}^{(\ell)} \right) \right) \right]. \quad (35)$$

Table 6. InternVL3-1B extended comparisons on DriveBench (%). Each row targets one capability; other entries are not applicable (“-”). For Ours (single-teacher), each reported score is obtained by distilling and evaluating that capability using its corresponding data only, consistent with the single-capability setting above.

Variant	Perception	Reasoning	Planning
CE + Full Attn (1)	42.46	–	–
CE + A_{t-v} (mid)	–	30.42	–
CE + Full Attn (ℓ_{pen})	–	–	51.47
CE + A_{t-v} (mid 2 → $\ell_{\text{pen}} - 1$)	–	31.43	–
CE + A_{t-v} (1), cosine	41.85	–	–
CE + Full Attn (mid), cosine	–	32.87	–
CE + A_{t-v} (ℓ_{pen}), cosine	–	–	51.76
Ours (single-teacher)	43.13	34.32	52.97
Ours (multi-teacher)	43.50	33.15	55.51

As shown in Table 6, we find that alternative attention choices are consistently weaker than our final single-teacher recipe on the targeted capability. For reasoning, expanding distillation to a non-overlapping intermediate range (Layer 2 to $\ell_{\text{pen}} - 1$) improves over the mid baseline, but it is still below our final reasoning recipe that covers a broader range from Layer 1 to ℓ_{pen} . This supports our layer-selection principle that reasoning supervision should leverage broad intermediate fusion layers, and that including the boundary layers helps better connect early perception cues with late-stage planning features. Finally, MSE attention matching is generally stronger than similarity-based matching in this setting, so we use MSE as the default attention distillation loss throughout Drive-KD.

Evaluation Example (Perception)



CAM.FRONT

Question: What is the moving status of object <c3,CAM.FRONT,0.4755,0.5231>? Please select the correct answer from the following options: A. Turn right. B. Turn left. C. Going ahead.

Model: GPT-5.1

Prediction (compressed):

Answer: C. Going ahead.

Explanation: Object c3 is the silver van located roughly in the center lane ahead. Its orientation aligns with the lane's straight arrow markings, and its motion appears to follow the lane forward rather than turning left or right....

Model: Ours (Drive-KD)

Prediction:

Final: A. Turn right.

Object: gray van

Position & orientation: relative to ego front, heading turning right

Environment: visible intersection with traffic signals and lane markings

Contextual evidence: the van's trajectory follows the right-turn lane, and its front wheels are angled right, ...

Evaluator: DeepSeek-V3.2

Ground Truth: A

DeepSeek grading for GPT-5.1:

1. Answer Correctness (50 points): 0
2. Object Recognition (10 points): 5
3. Object Location and Orientation (15 points): 5
4. Environmental Condition Awareness (15 points): 0
5. Clarity of Reasoning (10 points): 8

Total Score: 18

Brief Summary: ...

DeepSeek grading for Ours (Drive-KD):

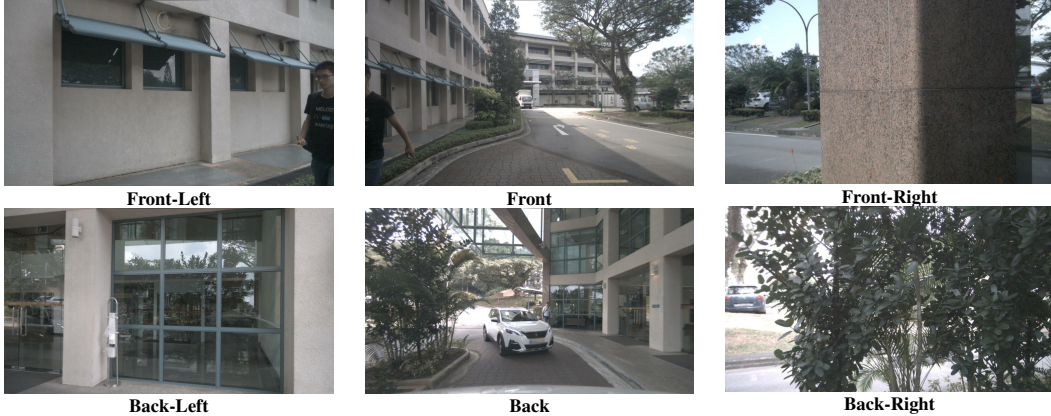
1. Answer Correctness (50 points): 50
2. Object Recognition (10 points): 5
3. Object Location and Orientation (15 points): 10
4. Environmental Condition Awareness (15 points): 10
5. Clarity of Reasoning (10 points): 8

Total Score: 83

Brief Summary: The predicted answer correctly identifies the moving status as "Turn right" (A), matching the ground truth, earning full correctness points. Object recognition is partially accurate: the prediction describes a "gray van," but the ground truth specifies a "white sedan," leading to a deduction for misidentification of color and vehicle type, though both are vehicles in a similar context. Location and orientation are well described with details like "relative to ego front, heading turning right" and mention of lane markings and trajectory, ...

Figure 12. Illustration of our evaluation process on a DriveBench perception question. For readability, the model responses and DeepSeek justifications are compressed while preserving the grading structure and key reasons.

Evaluation Example (Reasoning)



Question: Predict the behavior of the ego vehicle. Please select the correct answer from the following options: A. The ego vehicle is going straight. The ego vehicle is not moving. B. The ego vehicle is steering to the right. C. ... D.

Model: GPT-5.1

Prediction (compressed):

Answer: B.

- In the front view, the upcoming lane curves to the right, and the ego vehicle appears aligned with that curve, indicating a right steering input.
- Several pedestrians are very close to the vehicle, and another car is close behind in the back view....

Model: Ours (Drive-KD)

Prediction:

Final: A.

Support: The ego vehicle is positioned in the center of the lane with no visible steering or trajectory deviation; the road ahead is clear and straight, and there are no indications of motion blur or speed change in the surrounding environment....

Evaluator: DeepSeek-V3.2

Ground Truth: A

DeepSeek grading for GPT-5.1:

1. Answer Correctness (50 points): 0
2. Behavioral Understanding and Detail (15 points): 0
3. Reasoning and Justification (15 points): 0
4. Contextual Relevance (10 points): 0
5. Clarity and Grammar (10 points): 10

Total Score: 10

Brief Summary: ...

DeepSeek grading for Ours (Drive-KD):

1. Answer Correctness (50 points): 50
2. Behavioral Understanding and Detail (15 points): 15
3. Reasoning and Justification (15 points): 15
4. Contextual Relevance (10 points): 10
5. Clarity and Grammar (10 points): 10

Total Score: 100

Brief Summary: The predicted answer exactly matches the correct answer (A), earning full points for correctness. The explanation accurately captures the ego vehicle's behavior of going straight and not moving, with clear details about lane positioning, lack of steering deviation, and environmental cues like a clear road and no motion blur. Reasoning is logical and well-supported ...

Figure 13. Illustration of our evaluation process on a DriveBench reasoning question. For readability, the model responses and DeepSeek justifications are compressed while preserving the grading structure and key reasons.

Evaluation Example (Planning)



CAM_BACK

Question: What actions could the ego vehicle take based on <c1,CAM_BACK,0.5073,0.5778>? Why take this action and what's the probability?

Model: GPT-5.1

Prediction (compressed):

Object: <c1,CAM_BACK,0.5073,0.5778>
(passenger car), behind the ego and closing.

Action: maintain current lane; keep speed smooth; avoid hard braking.

Reason: close follower → reduce rear-end risk; suggests cautious anticipation for potential cross-traffic / distant vehicles...

Probability: 0.8.

Final: maintain lane with smooth, anticipatory speed control.

Model: Ours (Drive-KD)

Prediction:

Object: <c1,CAM_BACK,0.5073,0.5778> (gray sedan), relative to ego: back-left.

Action: keep going at the same speed

Reason: The gray sedan is in the adjacent lane moving straight ahead with no indication of braking or lane change; the road is clear ahead and no obstacles or hazards are visible in the immediate vicinity.

Probability: high

Final: keep going at the same speed to maintain safe clearance and traffic flow

Evaluator: DeepSeek-V3.2

Ground Truth: keep going at the same speed; no safety issue; probability high.

DeepSeek grading for GPT-5.1:

1. Action Prediction Accuracy (40 points): 30
2. Reasoning and Justification (20 points): 12
3. Probability or Confidence Level (15 points): 10
4. Contextual Awareness and Safety Considerations (15 points): 10
5. Conciseness and Clarity (10 points): 8

Total Score: 70

Brief Summary: ...

DeepSeek grading for Ours (Drive-KD):

1. Action Prediction Accuracy (40 points): 40
2. Reasoning and Justification (20 points): 20
3. Probability or Confidence Level (15 points): 15
4. Contextual Awareness and Safety Considerations (15 points): 15
5. Conciseness and Clarity (10 points): 10

Total Score: 100

Brief Summary: The predicted answer correctly identifies the action as 'keep going at the same speed,' matching the ground truth exactly. The reasoning is clear, logical, and aligns with safety considerations, noting the absence of immediate hazards and the sedan's stable behavior in an adjacent lane. The probability is appropriately stated as 'high,' consistent with the ground truth's 'high' probability. ...

Figure 14. Illustration of our evaluation process on a DriveBench planning question. For readability, the model responses and DeepSeek justifications are compressed while preserving the grading structure and key reasons.